VTT Technical Research Centre of Finland

HOR Activity of Pt-TiO2-Y at Unconventionally High Potentials Explained

Geppert, Timon N.; Bosund, Markus; Putkonen, Matti; Stühmeier, Björn M.; Pasanen, Antti T.; Heikkila, Pirjo; Gasteiger, Hubert A.; El-Sayed, Hany A.

Published in:
Journal of the Electrochemical Society

DOI:
10.1149/1945-7111/ab90ae

Published: 05/01/2020

Document Version
Publisher's final version

Journal of The Electrochemical Society

HOR Activity of Pt-TiO_{2-Y} at Unconventionally High Potentials Explained: The Influence of SMSI on the Electrochemical Behavior of Pt

Journal of The Electrochemical Society, 2020 **167** 084517

HOR Activity of Pt-TiO_{2-Y} at Unconventionally High Potentials Explained: The Influence of SMSI on the Electrochemical Behavior of Pt

Timon N. Geppert,[1,z] Markus Bosund,[2] Matti Putkonen,[3,a] Björn M. Stühmeier,[1] Antti T. Pasanen,[3] Pirjo Heikkilä,[3] Hubert A. Gasteiger,[1,*] and Hany A. El-Sayed[1]

[1]*Technical University Munich, Department Chemistry and Catalysis Research Centre, Chair of Technical Electrochemistry, 85748 Garching, Germany*
[2]*Beneq Oy, 02200 Espoo, Finland*
[3]*VTT Technical Research Centre of Finland Ltd., FIN-33101 Tampere, Finland*

The formation of strong metal support interactions (SMSI) is known for many metal/metal oxide systems and its consequences are well established in the field of heterogeneous catalysis, but this knowledge has only been recently transferred to the field of electrocatalysis. In this study, Pt was deposited via atomic layer deposition (ALD) onto TiO_{2-Y}, which allowed a good control of the particle size through the number of ALD cycles. During the ALD process, a thin-film of reduced titania is formed on the Pt surface, which leads to SMSI effects. With increasing Pt particle size, the fraction of the titania-covered Pt surface decreases. As a result, the extent of platinum oxide formation in cyclic voltammetry (CV) measurements scales with the size of the Pt particles. The influence of these thin titanium oxide films, which cover the Pt surface, on the catalytic behavior with respect to oxygen reduction reaction (ORR), hydrogen oxidation reaction (HOR), CO oxidation and oxygen evolution reaction (OER) is investigated by using an RDE setup. The covering TiO_X thin-films reduce the ability to catalyze ORR, OER and CO oxidation, while it does not influence the HOR and Pt H-UPD formation. These findings indicate that proton and hydrogen transport are possible through the thin TiO_X film, while oxygenated species suffer from transport limitations through the thin-film. Due to this selective permeability, these materials are able to oxidize hydrogen well beyond 1.2 V_{RHE}.

 [DOI: 10.1149/1945-7111/ab90ae]

Manuscript submitted January 17, 2020; revised manuscript received May 3, 2020. Published May 15, 2020.

Supplementary material for this article is available online

A tremendous progress has been made in the development of proton exchange membrane (PEM) fuel cells (FCs) in the past decades and FC cars are now commercially available in small series. Mass-market penetration however is still not feasible due to several factors, including the high noble metal contents in the catalyst layers and the insufficient durability of the catalyst. Loss of catalyst active area during operation and carbon corrosion during start up and shut down (SUSD) of the FC system are key factors which determine the catalyst durability. When a fuel cell is shut down, a hydrogen/air front passes through the anode, which results in oxidation of the carbon black support on the cathode side.[1,2] The loss of only ten percent of the mass of carbon on the cathode can result in a catalyst layer structure collapse resulting in high transport resistances.[3] Mitigation of the damage induced by SUSD can either be achieved by engineering solutions, e.g. purging strategies which result in a hydrogen-containing gas within the stack after shut down, or by choosing a corrosion resistant catalyst support instead of carbon black. Therefore, metal oxides, carbides, and nitrides have been investigated intensively as potential supports, for example; tungsten carbide and oxide,[4,5] tin oxides,[6–8] as well as titanium carbides,[9] nitrides,[10] and oxides.[11–13]

It became evident from electrochemical studies with platinum/titanium oxide catalysts in the last few years that these materials show some unexpected behavior, namely depressed platinum oxide formation and oxide reduction in the voltammograms. In many cases, this behavior is not addressed by the authors, even though it is evident from the presented electrochemical data.[12,14–17] Shintani et al. brought forward the hypothesis of potential dependent conductivity changes due to adsorbed oxygen species.[15] Hayden and coworkers showed a correlation between particle size and electrochemical oxide formation of Pt deposited via physical vapor deposition (PVD) on titanium oxide.[18] This correlation only exists for smaller particles and above a certain threshold, the oxide formation remained constant. For very small particles, the oxide formation was nearly completely suppressed. The authors hypothesized lowered kinetics of the Pt/Pt-O redox couple with decreasing particle size to be responsible for this behavior. This depressed oxide formation in the cyclic voltammograms (CV) was not observed for Pt deposited via PVD on a carbon support.[19] Lately, Banham and coworkers addressed a reduction in oxide formation for a Pt/Nb-TiO_2 catalyst after voltage cycling. They suggested that the Pt surface gets covered by Ti or Nb leached from the support during voltage cycling, which would alter the electrochemical behavior of Pt.[20] The coverage of the Pt surface with a titanium oxide film was recently confirmed by Hsieh and coworkers, who linked the depressed oxide formation to the strong metal support interactions (SMSI) between Pt and the titanium oxide support.[21] Eckhard et al. also suggested the possibility of formation of a reduced titania thin-film on Pt particles, like in a SMSI system, to explain an observed decrease in ORR performance and Pt oxide formation. That was observed after performing accelerated stress tests (AST) on Pt/TiO_2 and Pt/TiO_2@CNT (titania-coated carbon nanotubes) catalysts.[22] The coverage of Pt by a thin-film of titania and its effects on the electrochemistry was also shown in a recent study from our group for a Pt/TiO_X catalyst.[23]

Interplay between noble metals like platinum group metals (PGM) and titanium oxide (or other partially reducible oxides), which enhances the catalytic activity towards gas phase hydrogenation, have been termed strong metal support interactions in the late 1970s.[24,25] This effect has been explained in the 1980s with the formation of reduced titania film on the noble metals surfaces.[26] However, in the field of fuel cell catalysis, only electronic effects of the SMSI have been brought forward to explain certain effects, e.g., enhanced stability of Pt particles towards voltage cycling and/or increased activity towards the oxygen reduction reaction (ORR).[11,13,27] No attention has been paid to the aspect of oxide coverage of the noble metal by the support oxide until the above mentioned recent studies were published.

*Electrochemical Society Fellow.
[a]Present address: Department of Chemistry, University of Helsinki, FI-00014 Helsinki, Finland.
[z]E-mail: timon.geppert@tum.de

The SMSI effect has generally been observed in heterogeneous catalysis after a reductive heat treatment in a hydrogen atmosphere at elevated temperatures (e.g., 500 °C). Along with an increased catalytic activity, a clear reduction of metal surface areas, measured by gas phase adsorption using hydrogen or carbon monoxide, has been noted as well. This effect can be reversed by the heat treatment of the catalyst in oxygen at elevated temperatures (e.g., 400 °C) followed by a reductive step at lower temperatures (e.g., 175 °C).[24] The formation of titanium oxide thin-films on platinum group metals was explained by the migration of Ti^{3+} ions onto the metal surface, which takes place during the reductive heat treatment.[26] The onset temperature of this effect was shown to be near 200 °C,[28] a reduction temperature which was also employed by Hsieh et al.[21] These oxide films covering the metal surfaces have been imaged by various microscopic methods.[21,23,29,30] Eckhard et al. observed that the losses in ORR activity were smaller when the lower vertex potential in the voltage cycling ASTs was raised from 0.4 V_{RHE} to 1.0 V_{RHE} or when the ASTs were conducted in oxygen (instead of nitrogen) saturated electrolyte. Therefore, they argued that the reductive environment during the ASTs is detrimental to the catalyst's activity, linking it with the reductive environment during SMSI formation.[22]

In the current study, we investigate the electrochemical behavior of platinum deposited on titanium oxide-covered carbon fibers, produced using the atomic layer deposition (ALD) technique. Suppressed oxide formation for Pt deposited via ALD on Nb doped TiO_2, albeit after a reductive heat treatment, has been shown without addressing the phenomenon.[14] ALD deposition of Pt for fuel cell application has been used in recent years by several groups, mostly using various carbon types as support materials.[31–33] Ideally, conformal thin-films can be produced in the ALD process, which is typically applied in semiconductor and electronics applications. In the case of noble metal ALD, the formation of extremely thin (<2 nm) continuous films is difficult,[34] but it can be used to control the particle size of noble metals by adjusting the number of ALD cycles which also controls the metal loading.[31,33–36] In this work we specifically investigate the interplay between Pt particle size and the extent of SMSI effects, in addition to examining the consequences of the formation of a reduced titanium oxide thin-film covering the catalyst surface on the performance towards typical electrochemical reactions such as the HOR, ORR, OER, and CO oxidation.

Experimental

Synthesis and physicochemical characterization.— *Synthesis of the catalyst support.*—Synthesis and in-depth analysis of the oxide support has recently been described elsewhere[37] and is given briefly here. Polyacrylonitrile fibres sheets were electrospun using N,N-dimethylformamide (DMF) as solvent. The sheets were first oxidized at 270 °C in air, followed by carbonization in nitrogen (5.0) atmosphere at 1500 °C. TiO_2 films were deposited by ALD, using a Picosun R-200, onto carbonized sheets at 175 °C. Stop-flow mode was used in order to ensure sufficient diffusion time of the precursors through the fiber mat. $TiCl_4$ and H_2O (kept at 18 °C) were used as precursors. After deposition, the ~60 nm thick oxide film was annealed at 700 °C in reducing gas (4 % H_2 in Ar) for 120 min to obtain a crystalline and more conductive film on the fibrous carbon support. Throughout this manuscript, the support is labeled as TiO_{2-Y}, due to a partial reduction of the oxide during the annealing treatment.

Pt deposition.—Pt was deposited via ALD using trimethyl (methylcyclopentadienyl)platinum(IV) ((MeCp)$PtMe_3$) (99 %, 99.999 %-Pt, Puratrem grade, Strem Chemicals, used as received) and O_2 as precursors. The ALD reactor (Beneq TFS 200) was kept at 300 °C and 1 mbar and constantly flushed with 300 sccm N_2 (5.0 or higher) during all steps of operation. The Pt precursor was kept at 80 °C during deposition. After the oxide-covered fiber mats were loaded into the cold reactor, the reactor was heated, which took approximately 60 min. The precursors were pulsed using the reduced-flow technique where the pump speed was reduced after each precursor pulsing. The ALD cycles were performed as follows: (MeCp)$PtMe_3$ was dosed into the reactor using four micro-pulses (0.5 s load time, 4 s release time, followed by 1 s line purge with N_2), followed by 70 s reactor purge (with N_2). Oxygen was dosed with four micro-pulses (1 s O_2 flow, 1 s wait time). Excess oxygen and byproducts were removed by purging the reactor for 70 s (with N_2). Three different samples prepared via 10, 25, and 50 Pt ALD cycles were obtained. These samples are named throughout the manuscript according to the number of Pt ALD cycles as 10#Pt, 25#Pt, and 50#Pt. A 60 $\%_{wt.}$ Pt catalyst on a high surface area carbon supported (further referred to as 60 $\%_{wt.}$ Pt/C) was used in CV experiments for comparison (Johnson Matthey Fuel Cell) and a 5 $\%_{wt.}$ Pt on high surface area carbon supported (referred to as 5 $\%_{wt.}$Pt/C) (TEC10V05E, Tanaka Kikinzoku Kogyo) was used in HOR, ORR and CO oxidation experiments for comparison.

Physicochemical characterization.—Transmission electron microscopy (TEM) measurements were conducted by depositing samples directly from diluted RDE inks (see below) onto carbon coated copper grids (Cu, 400 mesh, formvar-carbon film, Science Services). The obtained samples were analyzed using a Philips CM100EM with an acceleration voltage of 100 kV and a resolution of 0.5 nm.

Electrochemical characterization.— *Preparation of catalyst inks and films.*—Inks were prepared by weighing the catalyst webs, crushing the web piece in a glass vial with a spatula and adding water (Milli-Q, 18 MΩ·cm, Merck Millipore) and isopropanol (IPA) (HPLC grade, Sigma-Aldrich) in the desired volume ratios. After cooling down the ink in an ice bath for 10 min, the ink was horn-sonicated (Branson Sonifier 250 W, double stepped micro-tip, 13 % amplitude, 0.7 s/0.4 s pulse on/off, 13 min pulse time) while keeping it in the ice bath. Before each coating procedure, the ink was sonicated in an ultrasonic bath (VWR) to ensure homogeneous distribution. Inks made from 10#Pt, 25#Pt and 50#Pt consisted of 20 % isopropyl alcohol (IPA) and 80 % water and varied in the composition between 1.75 and 2 mg of catalyst per ml of ink. Inks made of Pt/C catalysts were made by suspending the catalyst in pure dimethylformamide (DMF) at 1 mg of catalyst per ml of ink. All inks were ionomer free to avoid any catalyst poisoning. After depositing the desired amount of the ink on the glassy carbon disk (5 mm diam., Pine Research Inst.), the ink was either dried under an infrared lamp or at room temperature in air atmosphere, depending on which procedure gave the best film quality. The dried films were controlled by optical microscopy before and after the measurement to check the film quality as well as for signs of catalyst detachment, which was not observed for any measurements evaluated for this study. Before each measurement, the catalyst film was wetted with a drop of water prior to insertion into the electrolyte in order to remove trapped air within the pores of the coating.

Electrochemical testing.—Rotating ring disk electrode (RRDE) testing in acid electrolyte was performed in a custom-made three-compartment glass cell with a heating jacket. A custom-made reversible hydrogen electrode (RHE) was used as a reference electrode, while a Pt mesh (99.99 %) was used as a counter electrode. A Pine AFM rotator was used in combination with an Autolab PGStat 102 N potentiostat (Metrohm BV). A Julabo thermostat, filled with 18 MΩ·cm water to avoid cross contamination, was used to control the cell temperature by means of a heating jacket. All glassware was cleaned thoroughly before use by soaking for at least 24 h in piranha acid, followed by extensive rinsing with 15 MΩ·cm water, followed by 5 times boiling in 18 MΩ·cm water.

High purity gases (Ar 6.0, O_2 6.0, H_2 6.0 and CO 4.7) from Westfalen AG were used in this study. The electrolyte (0.1 M) was prepared from 60 $\%_{wt.}$ $HClO_4$ (Kanto Chem, Japan, reagent grade) using 18 MΩ·cm water.

Unless otherwise specified, the upper potential window in all experiments was limited to 1.2 V_{RHE}, while the lower potential was varied between 60 and 20 mV_{RHE} depending on the hydrogen evolution (HER) onset potential. Prior to any measurements, the catalyst films on the GC disk were electrochemically cleaned and stabilized in Ar-saturated electrolyte by conducting cyclic voltammetry (CV) up to 200 CVs at 200 mV s^{-1}, until stable CVs could be reproduced. Afterwards, the electrolyte was replaced, and CVs for catalyst characterization were recorded using the Autolab Scangen module, while polarization curves (ORR, HOR, CO oxidation) were measured using staircase voltammetry procedures. A polycrystalline platinum ring disc electrode (referred to as Pt(pc), 5 mm diameter, Pine Inst.) was used for comparison in OER measurements. To avoid contamination from gases due to bubbling of the electrolyte, the electrolyte was changed prior to any ORR measurements and also after measurements involving carbon monoxide oxidation. Impedance was measured to determine the high frequency resistance (HFR) to correct for the solution resistance.

All potentials reported in this paper are corrected for the HFR and referenced to the reversible hydrogen electrode scale (RHE). Respective potential windows, scan rates, and applied rotation rates are given in the text and figure captions.

Determination of the roughness factor (RF).—The roughness factor (rf) of the catalyst films is defined as the quotient of electrochemical surface area (ECSA) and the geometric area of the GC disk. The ECSA was determined from hydrogen underpotential deposition (H-UPD) at 100 mV s^{-1} as mean value of adsorption and desorption charge with 0.5 V_{RHE} as an upper potential limit and the lower vertex potential being adjusted in such a way that the combined hydrogen evolution/hydrogen adsorption current was equivalent to the local current maximum around 0.12 V_{RHE} in the negative going scan. The procedure is adapted from literature.[38]

Results and Discussion

Physical characterization.—Figure 1 shows TEM images of the three investigated Pt/TiO_{2-Y}/C ALD-catalysts, where it can clearly be seen that the Pt particles are deposited homogeneously on the oxide surface. Direct Pt deposition on the carbon fiber support is excluded here, as the ALD-deposited TiO_2 fully covers the carbon support as shown in a previous study.[37] The upper left image in Fig. 1 shows that the Pt nanoparticles have been successfully formed by 10 Pt ALD cycles (10#Pt) onto the oxide support. As the amount of Pt increases (25#Pt, Fig. 1 b), it can be seen that the Pt particles start to become more spherical and their coverage on the oxide surface increases. For the 50#Pt catalyst, the amount of Pt deposited on the support surface is sufficiently large that the Pt particles partially merge, forming band-like contiguous islands of Pt (Fig. 1 c). Island-type growth of Pt is a typical phenomenon in ALD and it usually takes from tens to hundreds of deposition cycles before a continuous film is formed.[34] As can be seen in the particle size distributions (Fig. 1 d), the average particle size for the 10#Pt catalyst is 4.2 ± 0.9 nm, while that for the 25#Pt catalyst is 6.2 ± 1.7 nm. The broader particle size distribution in case of the latter can be rationalized by merging of particles with increasing ALD cycles. Due to island-type shape of the Pt particles in the 50#Pt catalyst, no particle size distribution could be determined.

Electrochemical characterization.—Figure 2 shows the CVs of the three developed catalysts in addition to a carbon-supported Pt catalyst (Pt/C) that is used here as a reference. All current densities are normalized to the electrochemical active Pt surface area (ECSA) to allow for a better comparison of the different materials. To compare the electrochemical Pt features of the investigated catalysts with those of a standard Pt/C catalyst, a catalyst with a high Pt loading (60 $\%_{wt.}$ Pt) was chosen as a reference. The ratio of capacitive contribution of Pt over that of the carbon support for

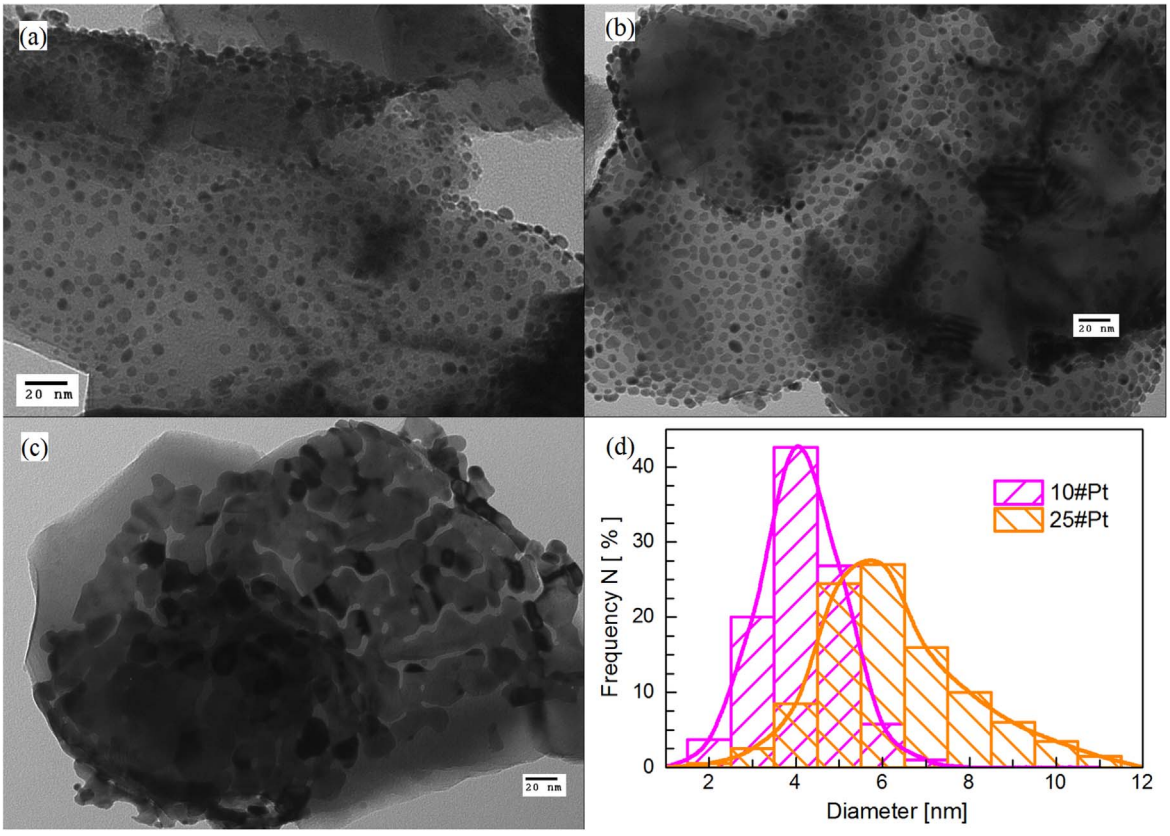

Figure 1. TEM images of titanium oxide-covered carbon fibres coated with platinum. Increasing number of Pt ALD cycles (10, 25 and 50, from (a) to (c)) indicates higher Pt loadings. Catalysts were named with the respective ALD cycles (10#Pt, 25#Pt and 50#Pt, from (a) to (c)). The catalyst dispersions used for RDE experiments were used to prepare the TEM samples. A particle size distribution for 10#Pt and 25#Pt is shown in (d), obtained from the these TEM images.

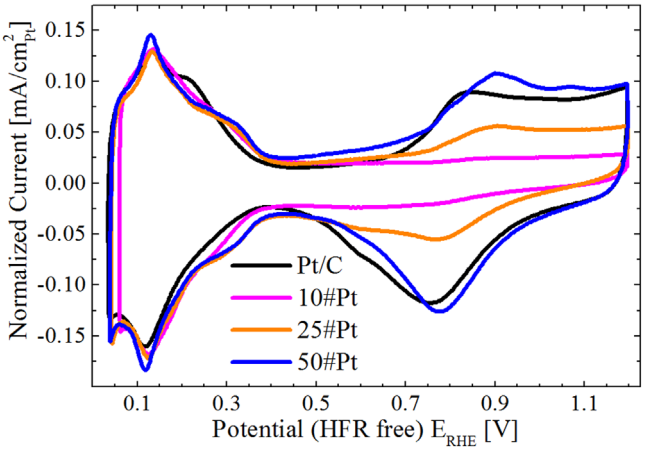

Figure 2. CVs of 10#Pt, 25#Pt and 50#Pt catalysts as well as of a 60 $\%_{wt.}$ Pt/C at 100 mV s^{-1} in Ar-saturated 0.1 M $HClO_4$. Currents are normalized to the Pt surface area determined from the H-UPD region.

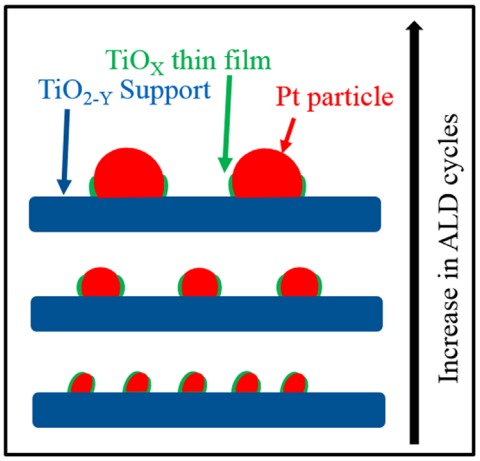

Figure 3. Schematic diagram of the correlation between the TiO_X film coverage and Pt particle size. The larger the number of Pt ALD cycles, the larger the Pt particle size, and the smaller the TiO_X surface coverage, and vice-versa.

this reference catalyst is similar to those of the investigated $Pt/TiO_{2-Y}/C$ catalysts.

The region below 0.5 V (H-UPD region), where hydrogen (as proton) is either adsorbed (negative going scan) or desorbed (positive going scan), shows similar features for all catalysts. Minor differences in the H-UPD features of the CV are most likely due to different ratios of Pt crystal facets.[39] Above 0.5 V (oxide region), where the Pt (hydr-)oxide formation and (hydr-) oxide reduction take place, the catalysts show distinct differences with respect to peak heights. For simplicity through most parts of this manuscript only the term "Pt oxide" is used, this incorporates as well the formation of Pt hydroxides. For typical Pt/C catalysts, it is known that currents for the H-UPD peaks and those for the oxide formation/reduction peaks increase simultaneously with increasing Pt loading,[19] and that the H-UPD peak currents are comparable to those of oxide formation/reduction peak currents. This behavior is an intrinsic property of platinum regardless of the type of support, as long as there is no interaction between the support and the platinum catalyst. For this case, the same behavior would have been expected for the ALD $Pt/TiO_{2-Y}/C$ catalysts. However, for these catalysts we found that with decreasing Pt ALD cycles—equivalent to a simultaneous decrease in Pt loading and particle size—the Pt oxide formation/reduction currents decrease significantly with respect to the H-UPD currents. For the catalyst with the highest Pt loading, 50#Pt, the oxide formation/reduction peaks exhibit currents comparable to those of the H-UPD peaks, and its CV resembles that of the Pt/C reference catalyst, while for the 25#Pt catalyst, the ratio of Pt oxide formation/reduction peak currents to H-UPD peak currents is lower compared to that of the 50#Pt catalyst. The current ratio is lowest for the 10#Pt catalyst, where almost no Pt oxidation/reduction peaks are visible. Depressed oxide formation/reduction features for an ALD Pt catalyst supported on titanium oxide have previously been shown by Du et al., but without addressing this phenomenon at all.[14]

As briefly mentioned in the introduction, Hsieh and coworkers attributed the depressed Pt oxide formation/reduction peaks of a Pt/TiO_2 catalyst to the presence of a SMSI.[21] This behavior was only observed after subjecting the Pt/TiO_2 catalyst to a reductive treatment under hydrogen atmosphere at 200 °C for one hour. It was shown that the reductive step resulted in the formation of a very thin film of TiO_X on the surface of the platinum, which then altered its electrochemical behavior. The removal of such an oxide film by HF etching resulted in a Pt CV with the same oxide formation/reduction peaks compared to that prior to the reductive treatment.[21] Therefore, depressed Pt oxide formation/reduction peaks compared to the H-UPD peaks seem to be correlated to the encapsulation of the Pt particles with a very thin TiO_X film.

Comparing the CV data obtained by Hsieh et al. with the CVs of the catalysts developed in this study indicates that the formation of a thin titanium oxide film on the Pt surface, attributed to the SMSI, has already occurred during the ALD process, as the developed $Pt/TiO_{2-Y}/C$ catalysts were not subjected to any reductive heat treatment after the synthesis, which leads to the change of the electrochemical properties of Pt in the $Pt/TiO_{2-Y}/C$ catalysts. Taking into consideration that with an increasing number of ALD cycles both the Pt loading and the Pt particle size increase, the CV results (Fig. 2) suggest that there is a correlation between the Pt particle size and the support interaction with the Pt catalyst through the TiO_X film. Figure 3 depicts a simple, hypothetical model shown to illustrate this correlation between the TiO_X coverage and particle size, which is inferred from the electrochemical data (Fig. 2), assuming that the TiO_X coverage is the only reason for the distorted Pt CVs for $Pt/TiO_{2-Y}/C$ catalysts. Our electrochemical data thus suggests that the larger the Pt particle size, the more the $Pt/TiO_{2-Y}/C$ catalyst behaves like a typical Pt catalyst, and the smaller the particle size, the more distorted the Pt CV becomes. This is attributed to the different coverage of the Pt surface with TiO_X for the three ALD catalysts: the fraction of the Pt surface covered with TiO_X is insignificant compared to the uncovered fraction for the largest Pt particle size catalyst (see upper part of Fig. 3), and for the smallest particle size, most of the Pt surface is covered with the thin TiO_X film (see lower part of Fig. 3). It has been suggested that those SMSI layers are in fact self-limited in thickness and only a few monolayers thick.[29,40] The existence of those layers has been proven previously, as shown for example in an overview for heterogeneous catalysts by Bernal et al.[30] For fuel cell relevant electrocatalysts, the formation of TiO_X films on the Pt surface upon reductive heat treatment of differently prepared $Pt/TiO_X/C$ catalysts has been proven as well by TEM.[21,23] Those studies do not indicate variations in film thickness. A similar behavior of reduced oxide formation has been described by Hayden and coworkers, as mentioned in the introduction, for CVD deposited Pt on TiO_2, which was rationalized by hindered kinetics for Pt oxide formation.[18] The coverage model presented here is supported by literature data.[41] The here investigated catalysts are not suitable to characterize the nature of the SMSI type thin-films, as the amount of SMSI-type reduced titania is much smaller compared to the amount of the ~60 nm thick TiO_{2-Y} oxide on carbon fiber support. This would require a study with designated model catalysts, as explained by Ross and Beard.[42] A more in-depth discussion on these matters is given in the supporting information (available online at stacks.iop.org/JES/167/084517/mmedia).

The formation of SMSI during the ALD process could be explained as follows. Since a titanium oxide thin-film coverage of

Pt can only be formed in the presence of reduced titanium dioxide with titanium ions Ti^{n+} ($n < 4$),[26,41] these ions either have to be formed prior to or during the Pt deposition. The TiO_{2-Y}-C support had been subjected to a treatment in 4% H_2/Ar at 700 °C prior to Pt deposition, which is required to increase the crystallinity and the support conductivity. During this process, the oxide has undergone partial reduction, forming Ti^{3+} and leading to an n-type-doped titanium oxide.[43] As mentioned in the experimental section, the material is labeled as TiO_{2-Y} to take the partial reduction during annealing into account. Since Pesty et al. reported evidence for the onset of encapsulation at 177 °C[41] and Hsieh et al. observed SMSI formation at 200 °C[21] as well, one can assume that the pre-existing Ti^{3+} ions are mobile enough during the Pt ALD process at 300 °C to migrate onto the freshly deposited Pt. Besides the partial reduction of the support during annealing, the reduction of Ti^{4+} to Ti^{n+} ($n < 4$) takes place during the ALD process itself at the applied process conditions, as shown in a recent study.[44] Since the focus on this paper is on the electrochemical properties of the Pt/TiO_{2-Y}/C catalysts, this latter pathway is explained in more detail in the SI.

Having discussed possible mechanisms for the formation of SMSI during catalyst synthesis, the formation of Pt H-UPD and Pt oxides in the presence of a titanium oxide thin-film on the platinum surface will be addressed.

$$Pt + H_2O \rightarrow Pt\text{-}OH + H^+ + e^- \quad [1]$$

$$Pt + OH^- \rightarrow Pt\text{-}OH + e^- \quad [2]$$

The electrochemical formation of Pt surface (hydr)-oxides can be described with the following reaction pathways, where the Pt hydroxide is either formed from adsorbed water (Eq. 1) or directly from a hydroxyl ion, provided by spontaneous water dissociation (Eq. 2). Hsieh et al. explained the depressed Pt oxide formation by assuming that the TiO_X thin-film blocks or hinders hydroxyl ions from reaching the Pt surface. The same reduced titania thin-film, however, was proposed to allow Pt H-UPD,[21] which is typically described for acid environment as follows (Eq. 3).

$$Pt + H^+ + e^- \rightarrow Pt\text{-}H \quad [3]$$

The proton is either available in the solution in the form of a hydronium ion or is formed in situ by water dissociation near the Pt surface. A reaction pathway via intermittent adsorption of water on the Pt surface (Eq. 4) is unlikely for a TiO_X covered Pt surface, as otherwise oxide formation should not be suppressed in the CV.

$$Pt + H_2O + e^- \rightarrow Pt\text{-}H + OH^- \quad [4]$$

Taking into consideration the depressed oxide formation compared to the H-UPD formation for 10#Pt and 25#Pt, it is reasonable to assume that the covering oxide thin-film allows, at least partially, proton diffusion and/or transport to the Pt surface for all the catalysts. Generally, proton and hydrogen insertion and diffusion in titanium oxide have been reported in the literature.[45–48] Ekström et al. deposited up to 18 nm of a titanium oxide film onto a Nafion 117 membrane and deposited a 3 nm Pt film on top of the titanium oxide film.[49] Using this electrode in a fuel cell setup did not alter the cell resistance in hydrogen atmosphere compared to a 3 nm Pt film deposited directly onto the Nafion 117 membrane. The authors explained these results by a proton conduction through the oxide itself in combination with proton conduction via the Grotthus mechanism along adsorbed water in the pores of the oxide. Since the covering oxide films for SMSI systems are typically thinner than two nanometers,[21,30] one can assume a film thickness of less than a few nanometers for the here investigated catalysts as well. Therefore, proton and hydrogen transport through these films should be feasible, explaining why the H-UPD is still possible even with an almost completely suppressed oxide formation.

In general, the activity of a Pt-based catalyst towards the oxygen reduction reaction (ORR) is directly related to the oxide formation/reduction on the Pt surface, where only metallic Pt is the catalytically active species for the ORR.[50] If the above-mentioned hypothesis of blocking the Pt surface with a thin oxide film is valid and the coverage of the Pt surface with the TiO_X is being inversely proportional to the Pt particle size, then there should be a correlation between the TiO_X coverage and the ORR activity. The suppressed platinum oxide formation has been explained earlier by hindered transport of either water or hydroxyl ions or both species through the TiO_X thin-film. As water is formed during the ORR (Eq. 5) and needs to desorb from the active sites, the TiO_X thin-film should have a negative influence on the ORR activity, as it hinders the water desorption.

$$O_2 + 4e^- + 4H^+ \rightarrow 2H_2O \quad [5]$$

Additionally the covering thin-film could simply block the transport of oxygen to the active sites on the Pt surface, hindering thereby the ORR. Based on the data presented here alone, this hypothesis can neither be confirmed nor ruled out. Thus, the highest TiO_X coverage (on small Pt particles) is expected to exhibit the poorest ORR activity and the lowest coverage (for large Pt particles) should exhibit the highest ORR activity within this category of Pt/TiO_{2-Y}/C catalysts. To investigate the effect of TiOx coverage on the ORR activity, the Pt/TiO_{2-Y}/C catalysts were tested for their activities towards the ORR and the results are shown in Fig. 4.

It is well evident from Fig. 4 that the onset of the ORR current shifts to lower overpotentials (more positive) with increasing number of ALD Pt cycles. Correlating with the trend of oxide formation, the onset of the ORR shifts positively with increasing the number of ALD Pt cycles, i.e., as the oxide features in the CV approach that of Pt/C. This shift of onset potential is not due to differences in Pt surface area on the electrode, as all measurements were conducted with similar Pt roughness factors (1.4–2.5 cm^2_{Pt}/cm^2_{geo}, see legend in Fig. 4). A 5%$_{wt.}$ Pt on Vulcan carbon was used as a reference, as with this catalyst very

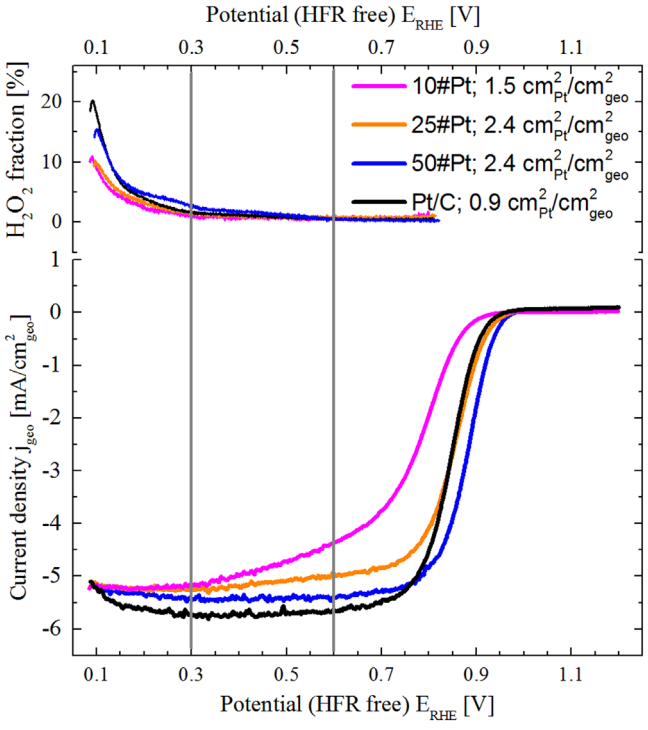

Figure 4. RRDE based ORR polarization curves of the ALD Pt/TiO_{2-Y}/C catalysts compared to a 5%$_{wt.}$ Pt/C as a reference. Roughness factors (in cm^2_{Pt}/cm^2_{geo}) of the electrodes are shown in the legend. Linear sweep polarization curves in anodic scan direction were recorded at 50 mV s^{-1} and 1600 rpm in O_2 sat. 0.1 M $HClO_4$. The vertical grey lines at 0.3 V_{RHE} and 0.6 V_{RHE} show the potential window for the calculation of the "*tilt*" (see text). The ring was held at 1.2 V_{RHE}.

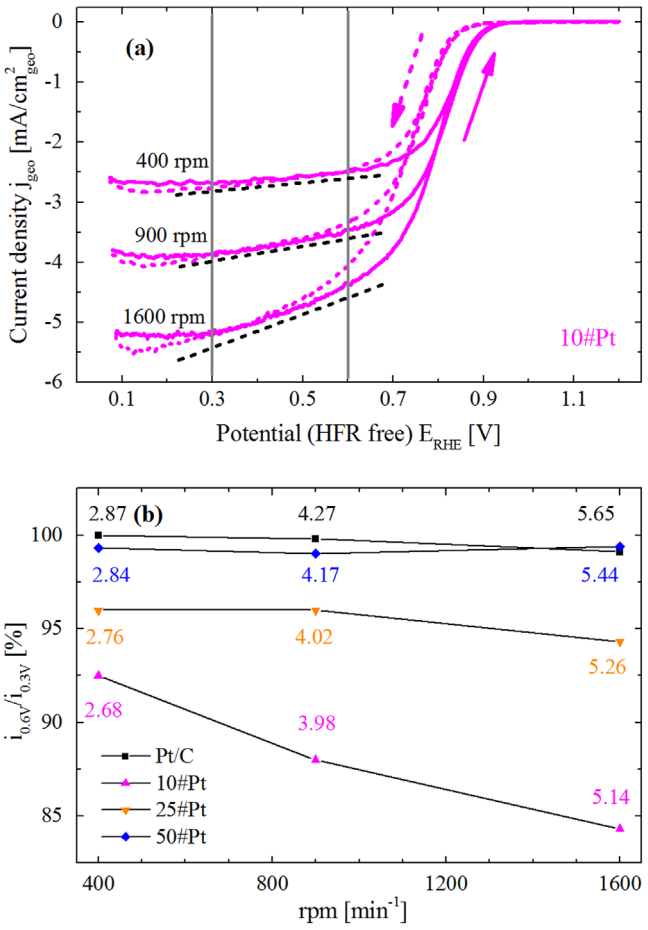

Figure 5. (a) ORR of 10#Pt at 400, 900 and 1600 rpm recorded at 50 mV s^{-1} in O_2 sat. 0.1 M $HClO_4$ at 25 °C. Scan direction is shown by magenta arrows. Vertical gray lines indicate the potentials used to determine the *tilt* (see (b)), dotted black lines are shown to qualitatively highlight the *tilt*. Roughness factors are given in the legend to Fig. 4. (b) Current ratio (*tilt*) $i_{0.6\ V}/i_{0.3\ V}$ of the anodic sweeps for all catalysts at 400, 900 and 1600 rpm with respective ORR currents at 0.3 V_{RHE} (marked in the figure) given in units of mA/cm$^2_{geo}$.

low Pt loadings can be achieved on the GC electrode while still obtaining complete coverage of the electrode surface with a catalyst film. In addition to the large overpotentials of the ORR, the shape of the polarization curves of 10#Pt and 25#Pt catalysts deviates significantly from those of Pt/C and of 50#Pt catalysts. Polarization curves of the latter catalysts behave as expected from a typical Pt catalyst, showing a sharp switch between mixed kinetic/diffusion regime to a purely diffusion limited regime with a flat current plateau between 0.7 V_{RHE} and 0.3 V_{RHE}. However, for the former two catalysts the polarization curves do not sharply switch from a mixed kinetic/diffusion regime towards a purely diffusion limited regime and a current plateau is not reached around 0.6 to 0.7 V_{RHE}. Instead current gradually increases with decreasing the potential down to 0.3 V_{RHE}. This current increase in a potential window at which a diffusion-limited current plateau is expected will be referred to as "*tilt*" from now on. It is defined as the ratio of current at 0.6 V_{RHE} to the current at 0.3 V_{RHE}. Since these polarization curves are recorded at 50 mV s^{-1}, adsorption of impurities from the electrolyte is excluded as a cause for such *tilt*. It is well established that the formation of H_2O_2 during oxygen reduction due to a sequential 2 + 2 electron reduction pathway could lead to a lower overall current in the diffusion-limited regime. It is also known for carbon supported Pt catalysts,[51] Pt model catalysts,[52] and for non-noble metal catalysts[53] that the hydrogen peroxide yield increases with decreasing catalyst loading. Since low catalyst loadings were used in this study, the *tilt* might be due to a high H_2O_2 formation in the relevant potential region. Therefore, the fraction of H_2O_2 (%) produced during the ORR measurements, derived from ring currents,[54] is reported here as well (see upper part of Fig. 4). If the *tilt* between 0.3 and 0.7 V_{RHE} in the ORR curves of the 10#Pt and the 25#Pt catalyst were due to a large fraction of the two-electron pathway, a large H_2O_2 fraction would be expected to occur around 0.7 V_{RHE} and should decrease with decreasing potential. However, the data in the upper panel of Fig. 4 show very low H_2O_2 fractions (below 5%) from 0.7 to 0.3 V_{RHE}, and the H_2O_2 fraction only starts to increase significantly as the H-UPD on Pt takes place, which is expected and in accordance with the literature.[51] Furthermore, the 10#Pt and 25#Pt catalysts generally form the lowest amount of peroxide, while Pt/C and 50#Pt show slightly higher H_2O_2 fractions. This clearly proves that the *tilt* is not a result of a high fraction of oxygen reduction via the two-electron pathway.

Having excluded peroxide formation as a reason for the *tilt*, the only reasonable explanation for the poor ORR activity of some of the Pt/TiO_{2-Y}/C catalysts is the limited number of active sites available for the ORR on the Pt surface due to the high fraction of coverage with the thin TiO_X film. As mass transport, represented by limiting currents, in an RDE experiment is defined by the rotation rate,[55] the ORR behavior for all catalysts at various rotation rates was investigated (see Fig. 5), whereby the kinetic limitations become more pronounced at high currents, i.e., at high rotation rates. The 10#Pt catalyst that exhibits the lowest Pt oxide formation/reduction and the steepest *tilt* is shown in Fig. 5a and a comparison of the *tilt* for the different catalysts—plotted as a ratio of currents at 0.6 V_{RHE} to those at 0.3 V_{RHE} at various rotation rates—is shown in Fig. 5b. The *tilt* in the polarization curve is, as expected, absent for both the Pt/C and the 50#Pt catalysts at all rotation rates (Fig. 5b). In the case of the 10#Pt and the 25#Pt catalysts, increasing *tilts* (shown as deviations from 100%) are observed with increasing rotation rates (Fig. 5b). These catalysts do not reach the limiting current at potentials above 0.3 V_{RHE}, especially not at the higher rotation rates. Since for the 10#Pt and the 25#Pt catalysts the platinum oxide formation/reduction is significantly depressed, these catalysts are assumed to have the smallest fraction of uncovered Pt and thus exhibit the lowest active surface area for the ORR. This low active area for the ORR leads to the appearance of *tilted* polarization curves due to kinetic limitations, which become more significant at higher rotation rates at which higher turnover rates are necessary.

It can be concluded so far that the poor ORR activity of some of the ALD Pt/TiO_{2-Y}/C catalysts is due to the thin-film of TiO_X that covers a large fraction of the Pt surface and most likely reduces the accessibility of the oxygenated species to/from the Pt surface. Eckhardt et al. suggested as well that the covered platinum surface cannot be accessed by oxygen, while protons can reach the Pt surface due to their high mobility.[22]

To further investigate this hypothesis of hindered accessibility of oxygenated species, the activity towards continuous CO oxidation was probed at various rotation rates (100, 400, and 1600 rpm). As the CO oxidation (see Eq. 6) requires oxygenated species to either adsorb on the Pt surface or at least diffuse to the Pt surface in proximity to the adsorbed CO, it is expected that this reaction will be most hindered on the 10#Pt, as we expect it to exhibit the largest fraction of TiO_X-covered Pt surface.

$$\text{Pt-CO} + H_2O \rightarrow \text{Pt} + CO_2 + 2H^+ + 2e^- \quad [6]$$

Figure 6 shows the continuous CO oxidation on 10#Pt, 25#Pt, 50#Pt, and Pt/C catalysts, with Pt/C showing the expected behavior with an initial sharp peak, which represents stripping of adsorbed CO in the form of CO_2, followed by a decrease towards a diffusion controlled limiting current depending on the rotation rate. The current decrease in the positive going scan is explained by a decreasing number of free Pt sites, as the coverage of Pt with surface (hydr-) oxide increases, and the higher currents in the negative going scans below 1 V_{RHE} is a result of increased active surface area due to the hysteresis of Pt surface oxide formation/

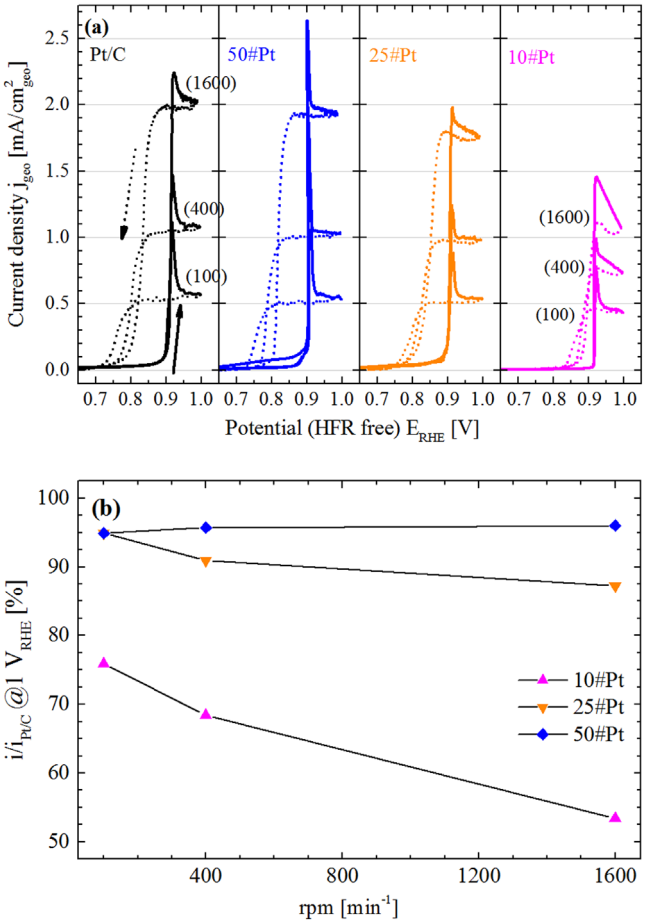

Figure 6. Continuous CO oxidation for 5%$_{wt.}$ Pt/C, 50#Pt, 25#Pt, and 10#Pt in 0.1 M $HClO_4$ (25 °C) at 100, 400, and 1600 rpm. (a) Linear sweep voltammograms at 10 mV s^{-1} between 0.06 and 1 V_{RHE}. To allow for a better comparison, only the relevant potential region above 0.6 V_{RHE} is shown. The scan direction is indicated by arrows, solid lines are used for positive going scans and dotted lines for negative going scans. Rotation rates are given in brackets for clarification. (b) Currents at 1.0 V_{RHE} from negative going scans normalized to the respective Pt/C currents at the same conditions are shown. Values below 100% indicate increasing kinetic limitations.

reduction. The 50#Pt catalyst shows a similar behavior to that of Pt/C, consistent with its similar CV and ORR activity. For the 25#Pt catalyst, the obtained diffusion-limited oxidation currents are similar to those of Pt/C and 50#Pt catalysts for 100 and 400 rpm, but the current in the plateau region at ~1 V_{RHE} deviates significantly at 1600 rpm, where it is much lower than that for Pt/C and 50#Pt catalysts. When the ALD Pt loading is further decreased (10#Pt), all limiting currents are significantly lower than those obtained on Pt/C and 50#Pt, including the limiting current obtained at 100 rpm. These findings demonstrate increasing kinetic limitations for the 25#Pt and the 10#Pt catalysts, as not enough active sites, i.e., uncovered Pt surface, are available, as discussed for the ORR before. These limitations are relevant especially at higher rotation rates, where larger currents are expected, and are in accordance with increasing coverage of the Pt surface with a TiO_x thin-film as the number of ALD cycles is reduced (corresponding to smaller particle size). The CO oxidation could be as well limited by hindered diffusion of CO through the TiO_X thin-film, in addition to the obstacles of hindered diffusion of oxygenated species. CO could be ad- or chemisorbed by the thin-film or physically blocked due to its molecular size. Based on the data presented here alone, this hypothesis can neither be confirmed nor ruled out.

The results presented so far show that the catalytic performance for the ORR or for the continuous CO oxidation is hindered by the

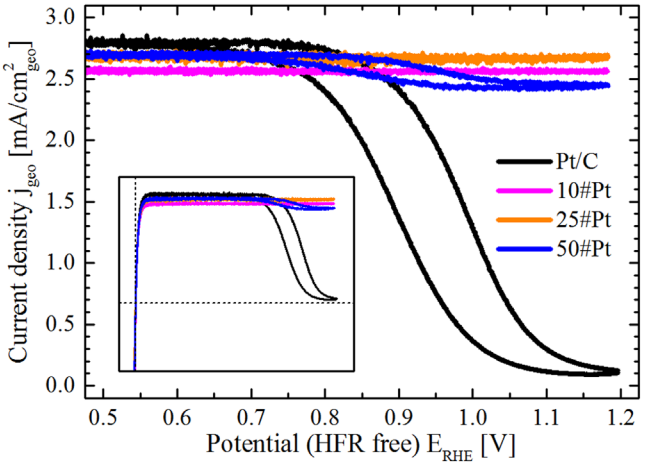

Figure 7. HOR in H_2 sat. 0.1 M $HClO_4$ at 25 °C and 1600 rpm at 10 mV s^{-1}. The inset shows the full potential range (−0.05 V_{RHE} to 1.25 V_{RHE}), while the main figure is limited to the most relevant potentials (above 0.45 V_{RHE}).

coverage of the Pt surface with a TiO_x thin-film, and that only the Pt-H adsorption/desorption is not strongly influenced by the TiO_x thin-film. The hindered Pt oxide formation may as well influence the hydrogen oxidation reaction, which is known to take place on Pt but not on Pt oxide. In other words, the formation of the platinum surface oxide represents the upper limit of the potential window in which a Pt catalyst can oxidize hydrogen.[50,56,57] Since the Pt oxide formation was found to be depressed for some of the Pt/TiO_{2-Y}/C catalysts, we investigated the hydrogen oxidation activity for these materials at potentials where Pt is usually covered with a Pt surface oxide layer and the HOR activity is expected to vanish (Fig. 7). The commercial Pt/C catalyst shows the expected activity decrease once the oxide formation on Pt initiates, viz., positive of around 0.8 V_{RHE}, while the Pt/TiO_{2-Y}/C catalysts exhibit HOR activity which remains high enough to result in only marginal (50#Pt) or no (10#Pt and 25#Pt) deviations from the diffusion-limited current density up to 1.2 V_{RHE} (~2.7 mA cm$^{-2}_{geo}$ at 1600 rpm[23]). Since the latter two show strongly hindered oxide formation, a correlation between the observed high HOR activity and the absence of Pt oxide at high potential can be established. As the 50#Pt catalyst shows oxide features that are very similar to those of a conventional Pt/C catalyst, a significant current decrease above 0.8 V_{RHE} would be expected; the observed small decrease in HOR activity from the diffusion-limited current can be explained by the fact that still a small fraction of the Pt surface is covered by the TiO_X thin-film. Additionally, next to the large Pt islands of the 50#Pt catalyst, some small isolated Pt particles (similar to those on 10#Pt and 25#Pt catalysts) were found as well (not shown in the TEM images above). Due to the extremely fast HOR kinetics with exchange current densities of ≈100 mA cm$^{-2}_{Pt}$,[58] these few particles, most likely covered with a TiO_X thin-film, might be sufficient to maintain high HOR currents even above 0.8 V_{RHE}. Banham et al. also reported unexpected hydrogen oxidation activities above 0.8 V_{RHE} for Pt/$NbTiO_2$ catalysts with depressed oxide formation,[20] as did Eckhard and coworkers in their study for a Pt/TiO_2/CNT catalyst,[22] whereby both catalysts exhibited a similar depressed oxide formation. The latter authors suggested an overgrowth of Pt by reduced TiO_X as a possible explanation of the observed phenomenon. In a previous study from our group, hydrogen oxidation currents up to 1.5 V_{RHE} were reported as well for Pt/TiO_X/C catalysts after a reductive heat treatment.[23] The reported CVs of membrane electrode assemblies (MEA) made from Pt supported on doped TiO_2 or TiN in the publications from Shintani et al. clearly show—owing to low applied scan rates and therefore low pseudo-capacitive currents—HOR currents as a result of hydrogen crossover

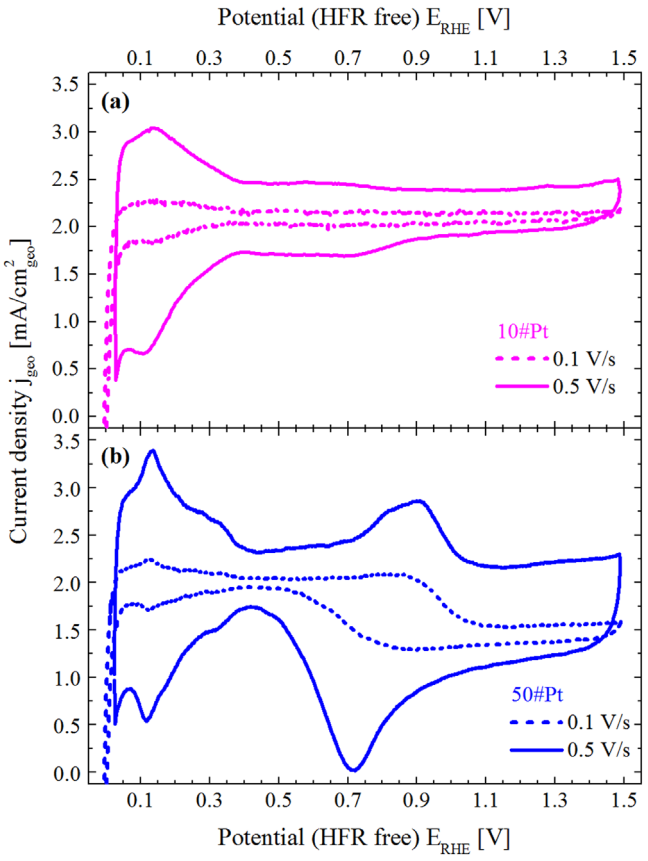

Figure 8. CVs of (a) 10#Pt (magenta) and (b) 50#Pt (blue) in H_2 sat. 0.1 M $HClO_4$ at 25 °C and 900 rpm. Recorded with a scan rate of 100 mV s^{-1} (dotted) and 500 mV s^{-1} (solid).

in the MEA.[10,15] Although the potential window was limited to 1.0 V, it can still be seen that the HOR currents for the reference Pt/C MEAs decrease at these potentials, while the TiO_2 or TiN supported catalysts allowed a constant HOR current. Although this phenomenon has been observed in those previous studies, it had not been discussed/interpreted in detail, and the correlation to suppressed Pt oxide formation is yet to be understood.

The correlation between oxide formation and hydrogen oxidation activity is demonstrated in Fig. 8 showing the voltammograms in a H_2 saturated $HClO_4$ electrolyte of 10#Pt and 50#Pt catalysts up to 1.5 V_{RHE} with scan rates of 100 mV s^{-1} and 500 mV s^{-1}. Owing to the presence of H_2, the voltammetric currents are upshifted by the value of the limiting current density at 900 rpm (viz., by ~2 mA cm^{-2}_{geo} at 900 rpm[23]). For the 50#Pt catalyst with the larger Pt particles and a minor fraction of TiO_X covered Pt surface, the decrease in HOR current density above 0.8 V_{RHE} coincides with a Pt surface oxide formation, most clearly visible at the fast scan rate of 0.5 V s^{-1} that magnifies capacitive currents (Fig. 8b). On the other hand, for the 10#Pt catalyst with small Pt particles and a high coverage of Pt with the TiO_X thin-film, neither visible decrease in HOR current nor any Pt surface oxide features are observed (Fig. 8a). This is remarkable, considering that at the upper potential vertex of 1.5 V_{RHE} a normal Pt surface is completely covered with surface oxide and inactive for the HOR. The TiO_X thin-films which (partly) cover the platinum surface in the here-investigated materials must thus be permeable for molecular hydrogen, as otherwise the HOR activity above 1.2 V_{RHE} cannot be explained. Molecular hydrogen uptake and diffusion in TiO_2 are known, as discussed above, and hydrogen diffusion coefficients in TiO_2 have been reported to be two orders of magnitude higher than those for proton diffusion.[59] However, the proton diffusion must still be sufficiently

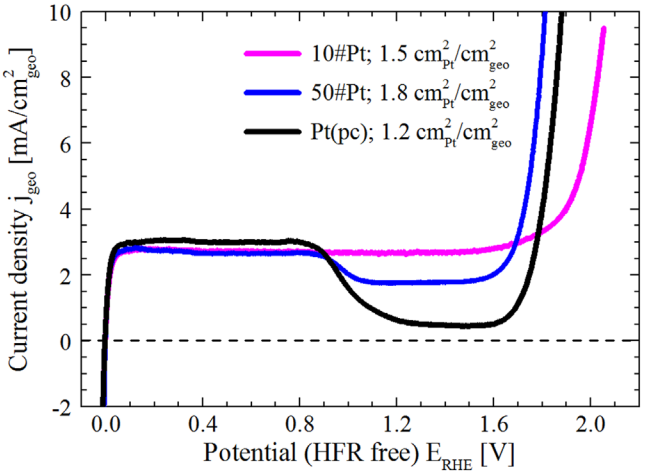

Figure 9. Combined HOR/OER sweeps of 10#Pt (magenta), 50#Pt (blue), and Pt(pc) as a reference (black line) in H_2 sat. 0.1 M $HClO_4$ at 25 °C, 1600 rpm and 100 mV s^{-1}. Roughness factors in cm^2_{Pt}/cm^2_{geo} are given as well. Only positive going scans are shown.

large, as the measured HOR currents for the $Pt/TiO_{2-Y}/C$ catalysts do not deviate from those recorded with a polycrystalline Pt disk (data not shown). Were the proton diffusion a limiting step, the measured HOR currents would be lower than those of a Pt disk. Therefore our data suggest that the TiO_X thin-films allow both HOR and HER (see (inset) of Fig. 7) at high rate, while they prevent the Pt oxide formation.[23]

Besides the formation of SMSI type TiO_X thin-films partially covering the Pt surface, the formation of a Schottky barrier between Pt and TiO_2 was also considered by the authors of this paper to explain the suppressed oxide formation. Shintani et al. suggested electronic effects to explain the reduced oxide formation in a $Pt/Ta_XTi_{1-X}O_2$ catalyst,[15] refering to an earlier study about a Pt/TiO_2 Schotty diode.[60] Detailed discussion on how the observed electrochemical behavior could be explained by the Schottky barrier is found in the SI. However, we argue that the data presented here cannot be rationalized by the Schottky barrier as the determining element for the electrochemical behavior of our $Pt/TiO_{2-Y}/C$ catalysts: If the hypothesis of a Schottky junction were correct, an increase in Pt oxide formation in the presence of hydrogen should occur, as the interaction of hydrogen with a Schottky junction would reduce the barrier height.[61] However, this is clearly not the case and the HOR current proceeds at high potential while the Pt oxide formation is still depressed, as can be seen in Fig. 8a.

The influence of the TiO_X thin-film on the Pt oxide formation by (partially) covering the Pt surface may also affect the oxygen evolution (OER) activity of these catalysts, as either the reaction of water or a hydroxyl ion (oxygenated species) is involved in the OER during the intermediate step.[62] A hindered platinum oxide formation should therefore result in higher OER overpotentials. To confirm this hypothesis, the OER was investigated in a hydrogen-saturated electrolyte in order to observe the limits of the hydrogen oxidation ability as well (Fig. 9). Both 10#Pt and 50#Pt catalysts behave up to 1.5 V_{RHE} as discussed earlier and the roughness factors (rf) for the two catalysts were very similar (1.5 cm^2_{Pt}/cm^2_{geo} for the former, 1.8 cm^2_{Pt}/cm^2_{geo} for the latter). For the 10#Pt catalyst, the current remains close to the diffusion-limited HOR current density up to 1.85 V_{RHE} (Fig. 9, magenta line), above which a steep current increase takes place due to the onset of the OER. Compared to polycrystalline Pt (Fig. 9, black line, roughness factor 1.2 cm^2_{Pt}/cm^2_{geo}), the 10#Pt catalyst shows a significantly delayed OER by ~130 mV, albeit having a bit higher rf than the Pt(pc) electrode. In the case of the less TiO_X covered Pt surface, 50#Pt, the OER behavior is similar to that of polycrystalline Pt (Fig. 9). The potential shift of ~80 mV could be due to the slightly higher rf of the electrode with the 50#Pt catalyst. This is

expected as for the 50#Pt catalyst there is a significant fraction of the Pt surface that is not covered with a TiO_X film. The OER behavior shown here suggests that the OER overpotential scales inversely with the material's ability to form Pt oxide. At currents of 5 mA cm^{-2}_{geo}, 10#Pt shows an overpotential of ca. 200 mV compared to 50#Pt, which is reasonable as 10#Pt shows significantly lower Pt oxide formation. It is remarkable that the hydrogen oxidation activity remains constant until the onset of the OER, and is most likely running in parallel to the OER on different active sites.

Conclusions

In this study we have investigated the electrochemical behavior of Pt supported on titanium oxide. The TiO_{2-Y}/C support was prepared by coating a carbonized electro-spun PAN fiber mat with TiO_2 via ALD, followed by a heat treatment in reducing atmosphere to increase crystallinity and conductivity. The deposition of Pt via ALD onto the titanium oxide support was shown to lead to the formation of a strong metal support interaction between the Pt nanoparticles and the oxide support, established by creeping of reduced titania onto the Pt surface. This effect occurred despite the fact that a final heat treatment in reducing atmosphere was omitted. This SMSI thin-film on Pt influenced significantly the electrochemical behavior of this type of catalyst compared to typical supported Pt electrocatalysts.

The TiO_X-covered Pt surface of these Pt/TiO_{2-Y}/C catalysts display suppressed Pt oxide formation/reduction features in the cyclic voltammograms. We provided evidence that the suppression of the formation of Pt surface oxides, which was observed up to 1.5 V_{RHE}, is responsible for the high HOR activity well beyond 1 V_{RHE}. The HOR takes places up to the onset potential of the OER, in stark contrast to what is observed for polycrystalline or carbon supported platinum. With increasing number of Pt ALD cycles and therefore increasing Pt particle size, the fraction of TiO_X-covered Pt surface decreases. Therefore, the behavior of the catalyst with 50 ALD cycles resembles conventional Pt/C or a polycrystalline Pt disk, with the exception of a higher HOR activity above 1.2 V_{RHE}. At a smaller Pt particle size (i.e., with fewer ALD cycles), the Pt oxide formation is nearly completely suppressed.

Furthermore, these SMSI-type thin-films on the Pt surface increased the overpotentials towards the ORR and the OER and decreased the electrochemical activity for the CO oxidation. This suggests high permeability for protons and hydrogen through these thin-films and hindered permeability for H_2O/OH^- and CO. The formation of a Schottky barrier, which would explain the ORR currents at the same potentials at which only minor oxide formation currents were observed, would not be consistent with the overall observed electrocatalytical features, especially the still reduced Pt oxide formation in the presence of hydrogen.

The results also show that the ability to form Pt oxide facilitates the OER, as the OER overpotentials are significantly higher for the catalyst with a strongly suppressed oxide formation. These results suggest a potential use of this type of catalysts at the anode side of an electrolyzer, where cross-over hydrogen could be oxidized, or in fuel cells to mitigate damages due to local fuel starvation during SUSD on the anode side.

Acknowledgments

The authors gratefully acknowledge funding from the European Union FCH-JU FP7 project CATAPULT (GA #325268) for catalysts synthesis and for some of the electrochemical characterization. Matti Putkonen acknowledges funding from the Academy of Finland by the profiling action on Matter and Materials, grant no. 318913. The authors like to thank the group of Henrik Dietz at TUM for the use of their TEM and as well Ian Harkness and Jonathan Sharman at Johnson Matthey Fuel Cell for many helpful discussions during the Catapult project on these ALD catalysts.

ORCID

Timon N. Geppert https://orcid.org/0000-0001-8152-388X
Matti Putkonen https://orcid.org/0000-0002-4166-2890
Björn M. Stühmeier https://orcid.org/0000-0001-7713-2261
Hubert A. Gasteiger https://orcid.org/0000-0001-8199-8703
Hany A. El-Sayed https://orcid.org/0000-0002-8769-8258

References

1. C. A. Reiser, L. Bregoli, T. W. Patterson, J. S. Yi, J. D. Yang, M. L. Perry, and T. D. Jarvi, *Electrochem. Solid-State Lett.*, **8**, A273 (2005).
2. T. Mittermeier, A. Weiß, F. Hasché, G. Hübner, and H. A. Gasteiger, *J. Electrochem. Soc.*, **164**, F127 (2016).
3. H. A. Gasteiger, W. Gu, B. Litteer, R. Makharia, B. Brady, M. Budinski, E. Thompson, F. T. Wagner, S. G. Yan, and P. T. Yu, *Mini-Micro Fuel Cells*, ed. S. Kakaç, A. Pramuanjaroenkij, and L. Vasiliev (Springer, Dordrecht) p. 225 (2008).
4. M. Perchthaler, T. Ossiander, V. Juhart, J. Mitzel, C. Heinzl, C. Scheu, and V. Hacker, *J. Power Sources*, **243**, 472 (2013).
5. Z. Yan, W. Wei, J. Xie, S. Meng, X. Lü, and J. Zhu, *J. Power Sources*, **222**, 218 (2013).
6. S. Cavaliere, S. Subianto, I. Savych, M. Tillard, D. J. Jones, and J. Rozière, *J. Phys. Chem. C*, **117**, 18298 (2013).
7. K. Kakinuma, M. Uchida, T. Kamino, H. Uchida, and M. Watanabe, *Electrochim. Acta*, **56**, 2881 (2011).
8. J.-P. Suchsland, B. Klose-Schubert, D. Herein, T. Martin, C. Eickes, and M. Lennartz, *ECS Trans.*, **50**, 1659 (2013).
9. L. Yang, Y. C. Kimmel, Q. Lu, and J. G. Chen, *J. Power Sources*, **287**, 196 (2015).
10. H. Shintani, K. Kakinuma, H. Uchida, M. Watanabe, and M. Uchida, *J. Power Sources*, **280**, 593 (2015).
11. S. Sun, G. Zhang, X. Sun, M. Cai, and M. Ruthkosky, *Journal of Nanotechnology*, **2012**, 1 (2012).
12. A. Bauer, L. Chevallier, R. Hui, S. Cavaliere, J. Zhang, D. Jones, and J. Rozière, *Electrochim. Acta*, **77**, 1 (2012).
13. A. Kumar and V. Ramani, *ACS Catal.*, **4**, 1516 (2014).
14. Q. Du, J. Wu, and H. Yang, *ACS Catal.*, **4**, 144 (2014).
15. H. Shintani, Y. Kojima, K. Kakinuma, M. Watanabe, and M. Uchida, *J. Power Sources*, **294**, 292 (2015).
16. M.-C. Tsai, T.-T. Nguyen, N. G. Akalework, C.-J. Pan, J. Rick, Y.-F. Liao, W.-N. Su, and B.-J. Hwang, *ACS Catal.*, **6**, 6551 (2016).
17. D.-S. Kim, E. F. A. Zeid, and Y.-T. Kim, *Electrochim. Acta*, **55**, 3628 (2010).
18. B. E. Hayden, D. Pletcher, J.-P. Suchsland, and L. J. Williams, *Physical Chemistry Chemical Physics: PCCP*, **11**, 1564 (2009).
19. B. E. Hayden, D. Pletcher, J.-P. Suchsland, and L. J. Williams, *Physical Chemistry Chemical Physics: PCCP*, **11**, 9141 (2009).
20. D. Banham, S. Ye, A. O'Toole, A. Lemke, and E. Eisenbraun, *Nano Energy*, **27**, 157 (2016).
21. B.-J. Hsieh, M.-C. Tsai, C.-J. Pan, W.-N. Su, J. Rick, H.-L. Chou, J.-F. Lee, and B.-J. Hwang, *Electrochim. Acta*, **224**, 452 (2017).
22. M. Eckardt, C. Gebauer, Z. Jusys, M. Wassner, N. Hüsing, and R. J. Behm, *J. Power Sources*, **400**, 580 (2018).
23. B. M. Stühmeier, S. Selve, M. U. M. Patel, T. N. Geppert, H. A. Gasteiger, and H. A. El-Sayed, *ACS Appl. Energy Mater.*, **2**, 5534 (2019).
24. S. J. Tauster, S. C. Fung, and R. L. Garten, *J. Am. Chem. Soc.*, **100**, 170 (1978).
25. S. J. Tauster and S. C. Fung, *J. Catal.*, **55**, 29 (1978).
26. S. J. Tauster, *Acc. Chem. Res.*, **20**, 389 (1987).
27. T. T. van Ho, C.-J. Pan, J. Rick, W.-N. Su, and B.-J. Hwang, *JACS*, **133**, 11716 (2011).
28. D. N. Belton, Y. M. Sun, and J. M. White, *J. Am. Chem. Soc.*, **106**, 3059 (1984).
29. O. Dulub, W. Hebenstreit, and U. Diebold, *Phys. Rev. Lett.*, **84**, 3646 (2000).
30. S. Bernal, J. J. Calvino, M. A. Cauqui, J. M. Gatica, C. López Cartes, J. A. Pérez Omil, and J. M. Pintado, *Catal. Today*, **77**, 385 (2003).
31. E. Sairanen, M. C. Figueiredo, R. Karinen, A. Santasalo-Aarnio, H. Jiang, J. Sainio, T. Kallio, and J. Lehtonen, *Appl. Catalysis B*, **148–149**, 11 (2014).
32. Y.-C. Hsueh, C.-C. Wang, C.-C. Kei, Y.-H. Lin, C. Liu, and T.-P. Perng, *J. Catal.*, **294**, 63 (2012).
33. T. Shu, D. Dang, D.-W. Xu, R. Chen, S.-J. Liao, C.-T. Hsieh, A. Su, H.-Y. Song, and L. Du, *Electrochim. Acta*, **177**, 168 (2015).
34. H.-B.-R. Lee and S. F. Bent, *Chem. Mater.*, **24**, 279 (2011).
35. Y.-C. Hsueh, C.-C. Wang, C. Liu, C.-C. Kei, and T.-P. Perng, *Nanotechnology*, **23**, 405603 (2012).
36. V. R. Anderson, N. Leick, J. W. Clancey, K. E. Hurst, K. M. Jones, A. C. Dillon, and S. M. George, *J. Phys. Chem. C*, **118**, 8960 (2014).
37. M. Putkonen, P. Heikkilä, A. T. Pasanen, H. Rautkoski, L. Svärd, P. Simell, M. Vähä-Nissi, and T. Sajavaara, *Journal of Vacuum Science & Technology A: Vacuum, Surfaces, and Films*, **36**, 01A102 (2018).
38. R. N. Carter, S. S. Kocha, F. Wagner, M. Fay, and H. A. Gasteiger, *212th ECS Meeting Oct. 2007*ECS Transactions, **11**, 403 (2008).
39. D. Li et al., *Energy Environ. Sci.*, **7**, 4061 (2014).
40. D. R. Jennison, O. Dulub, W. Hebenstreit, and U. Diebold, *Surf. Sci.*, **492**, L677 (2001).
41. F. Pesty, H.-P. Steinrück, and T. E. Madey, *Surf. Sci.*, **339**, 83 (1995).
42. B. C. Beard and P. N. Ross, *J. Phys. Chem.*, **90**, 6811 (1986).

43. U. Diebold, *Surf. Sci. Rep.*, **48**, 53 (2003).
44. F. Grillo, H. van Bui, D. La Zara, A. A. I. Aarnink, A. Y. Kovalgin, P. Kooyman, M. T. Kreutzer, and J. R. van Ommen, *Small*, **14**, e1800765 (2018).
45. G. Betz, H. Tributsch, and R. Marchand, *J. Appl. Electrochem.*, **14**, 315 (1984).
46. J. B. Bates, J. C. Wang, and R. A. Perkins, *Phys. Rev. B*, **19**, 4130 (1979).
47. S. P. Jiang, *J. Mater. Chem. A*, **2**, 7637 (2014).
48. F. M. Vichi, *Electrochem. Solid-State Lett.*, **2**, 313 (1999).
49. H. Ekström, B. Wickman, M. Gustavsson, P. Hanarp, L. Eurenius, E. Olsson, and G. Lindbergh, *Electrochim. Acta*, **52**, 4239 (2007).
50. G. K. H. Wiberg and M. Arenz, *J. Power Sources*, **217**, 262 (2012).
51. M. Inaba, H. Yamada, J. Tokunaga, and A. Tasaka, *Electrochem. Solid-State Lett.*, **7**, A474 (2004).
52. A. Schneider, L. Colmenares, Y. E. Seidel, Z. Jusys, B. Wickman, B. Kasemo, and R. J. Behm, *Physical Chemistry Chemical Physics: PCCP*, **10**, 1931 (2008).
53. A. Bonakdarpour, M. Lefevre, R. Yang, F. Jaouen, T. Dahn, J.-P. Dodelet, and J. R. Dahn, *Electrochem. Solid-State Lett.*, **11**, B105 (2008).
54. T. Mittermeier, P. Madkikar, X. Wang, H. A. Gasteiger, and M. Piana, *J. Electrochem. Soc.*, **163**, F1543 (2016).
55. A. J. Bard and L. R. Faulkner, *Electrochemical Methods and Applications* (Wiley-Interscience, New York, London) (2000).
56. Y.-J. Deng, M. Arenz, and G. K. H. Wiberg, *Electrochem. Commun.*, **53**, 41 (2015).
57. C. M. Zalitis, D. Kramer, and A. R. Kucernak, *Physical Chemistry Chemical Physics: PCCP*, **15**, 4329 (2013).
58. J. Durst, C. Simon, F. Hasche, and H. A. Gasteiger, *J. Electrochem. Soc.*, **162**, F190 (2014).
59. G. C. Yu, *Phys. Stat. Sol. (A)*, **198**, 302 (2003).
60. S. Hirose, A. Nakayama, H. Niimi, K. Kageyama, and H. Takagi, *J. Electrochem. Soc.*, **158**, H261 (2011).
61. M. Cerchez, H. Langer, M. El Achhab, T. Heinzel, D. Ostermann, H. Lüder, and J. Degenhardt, *Appl. Phys. Lett.*, **103**, 33522 (2013).
62. E. Fabbri, A. Habereder, K. Waltar, R. Kötz, and T. J. Schmidt, *Catal. Sci. Technol.*, **4**, 3800 (2014).